A Continuum Phase Field Model for Fracture

R. Müller[1], C. Kuhn[1]
[1]*Department of Civil Engineering and Geodesy, Solid Mechanics, TU Darmstadt, Hochschulstr. 1, 64289 Darmstadt, Germany*

1 Introduction

A variational free-discontinuity formulation of brittle fracture was given by Francfort and Marigo [1], where the total energy is minimized with respect to the crack geometry and the displacement field simultaneously. The entire evolution of cracks including their initiation and branching is determined by this minimization principle requiring no further criterion. However, a direct numerical discretization of the model faces considerable difficulties as the displacement field is discontinuous in the presence of cracks.
A regularized approximation of the model, which is more suitable for a numerical treatment, has been presented by Bourdin in [2, 3]. The underlying theory of Γ-convergence is exposed e.g. in [4]. An additional field variable s is introduced to model changes in the stiffness of the material. In this work, we interpret the variable s as an order parameter of a phase field model with an evolution equation of the Ginzburg-Landau type, similar to earlier phase field models for fracture, e.g. [5, 6]. The application of a phase field approach to crack propagation is possible with some modifications, taking the irreversible character of crack propagation into account. The numerical implementation is performed with finite elements and an implicit time integration scheme. Crack propagation, branching, and initiation is observed in different numerical examples.

2 A phase field model for fracture

In Bourdin's regularized model, cracks are represented by a field variable s which is 1 if the material is undamaged and 0 if there is a crack. Thus s can be viewed as a damage parameter in elastic damage models. The total energy E of a linear elastic body with stiffness tensor $\mathbb{C}$ and crack resistance G depends on the displacement field $\boldsymbol{u}$ and the crack indicator s

$$E(\boldsymbol{u}, s) = \int_\Omega \underbrace{\frac{1}{2}(s^2+\eta)\,\boldsymbol{\varepsilon}(\boldsymbol{u}) : \mathbb{C}\boldsymbol{\varepsilon}(\boldsymbol{u}) + G\left(\frac{(1-s)^2}{4\epsilon} + \epsilon\,|\nabla s|^2\right)}_{=\Psi(\boldsymbol{u},s)} dV\,. \tag{1}$$

In Eq. (1) the potential of external loads is neglected for the sake of simplicity only. The first term in Eq. (1) is the elastic strain energy density. The infinitesimal strain tensor $\boldsymbol{\varepsilon}$ is related to the displacement field $\boldsymbol{u}$ by

$$\boldsymbol{\varepsilon}(\boldsymbol{u}) = \frac{1}{2}\left(\nabla\boldsymbol{u} + (\nabla\boldsymbol{u})^T\right)$$

and the elastic stresses $\boldsymbol{\sigma}$ are derived from the energy density Ψ by

$$\boldsymbol{\sigma} = \frac{\partial \Psi}{\partial \boldsymbol{\varepsilon}} = (s^2 + \eta)\mathbb{C}\,\boldsymbol{\varepsilon}\,.$$

The factor $(s^2 + \eta)$ models the stiffness loss between an undamaged ($s = 1$) and a broken material ($s = 0$). The term $\eta\,\mathbb{C}$ with $0 < \eta \ll 1$ is the residual stiffness if $s = 0$. For numerical reasons (stability) η may not be chosen too small. However, too large values for η overestimate the bulk energy in fractured zones. In the absence of volume forces, the equilibrium condition reads

$$\operatorname{div} \boldsymbol{\sigma} = 0\,. \tag{2}$$

The second term in Eq. (1) represents the surface/crack energy. The width of the transition area between undamaged solid and broken material is controled by the parameter ϵ which has the dimension of a length [7]. With ϵ tending to zero, the transition area turns into a sharp interface and the regularized energy converges to the original energy expression by Francfort and Marigo which is the same as in classical Griffith fracture mechanics.
Interpreting s as an order parameter of a phase field model, the evolution is governed by a Ginzburg-Landau type evolution equation which is derived from the energy density Ψ [8]:

$$\dot{s} = -M \cdot \frac{\delta \Psi}{\delta s} = -M \left(s\,\boldsymbol{\varepsilon} : \mathbb{C}\boldsymbol{\varepsilon} - 2\,G\,\epsilon\,\Delta s + \frac{1}{2}\frac{G}{\epsilon}(s-1) \right)\,, \tag{3}$$

where $M \geq 0$ is a mobility constant. Eq. (3) has to be slightly modified in order to take account of the irreversible character of crack propagation. Two different strategies to avoid crack healing are possible:

- either fix s, if it is close to 0,
- or set $\dot{s}$ to 0, if $\dfrac{\delta \Psi}{\delta s} < 0$, so that $\dot{s} \leq 0$ holds.

The first alternative is used in the simulations of section 4.

2.1 1D stationary problem

To get a better understanding of the meaning of ϵ, the 1D example of a bar of length $2L$ with a crack in the centre is analysed. Neglecting the elastic energy and considering a stationary problem Eq. (3) yields in

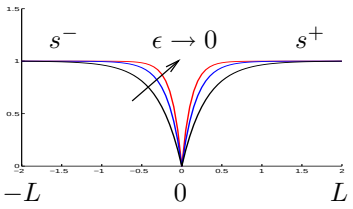

Figure 1: Cracked bar

$$-\frac{1}{2} = -\frac{s(x)}{2} + 2\epsilon^2 s''(x)$$

with $-L \leq x \leq +L$. The solution with a crack in the centre (at $x = 0$) is given by

$$s^{\pm}(x) = 1 - \cosh\left(\frac{x}{2\epsilon}\right) \pm \coth\left(\frac{L}{2\epsilon}\right) \sinh\left(\frac{x}{2\epsilon}\right)\,, \quad (+ \text{ for } x \geq 0, - \text{ for } x < 0).$$

Fig. 1 shows a plot of the solution $s(x)$ for different values of ϵ. Large values of ϵ smoothen the crack field, whereas the limit $\epsilon \to 0$ yields a discontinuous function which is 0 at $x = 0$ and 1 elsewhere.

Inserting the solution $s(x)$ into the expression for the surface energy, one can recover the crack resistance G letting $\epsilon \to 0$.

$$E^{\text{surf}} = G \int_{-L}^{+L} \frac{(1-s)^2}{4\,\epsilon} + \epsilon\, s'^2 dx = \frac{G}{2}\left(\coth\left(\frac{L}{2\epsilon}\right) + \coth\left(\frac{L}{2\epsilon}\right)\right) \overset{\epsilon\to 0}{=} G$$

3 Numerical implementation

The fracture model is implemented into a finite element framework with the displacements $\boldsymbol{u}$ and the order parameter s as nodal degrees of freedom. With virtual displacements $\delta\boldsymbol{u}$ and δs, the weak forms of Eq. (2) and Eq. (3) read

$$\int_\Omega \nabla\delta\boldsymbol{u} \cdot \boldsymbol{\sigma}\, dV = \int_{\partial\Omega_t} \delta\boldsymbol{u} \cdot \boldsymbol{t}_n^*\, dA \tag{4}$$

and

$$\int_\Omega \left[\delta s \frac{\dot{s}}{M} - \nabla\delta s \cdot \boldsymbol{q} + \delta s\left(s\boldsymbol{\varepsilon} : \mathbb{C}\boldsymbol{\varepsilon} + \frac{G}{2\epsilon}(s-1)\right)\right] dV = \int_{\partial\Omega_q} \delta s\, q_n^*\, dA \tag{5}$$

with $\boldsymbol{q} = -2G\,\epsilon\,\nabla s$. The boundary conditions for the stresses $\boldsymbol{\sigma}$ and for $\boldsymbol{q}$ are prescribed by $\boldsymbol{t}_n^*$ and q_n^*.

In a 2D setting using Voigt-notation - denoted by an underbar in the following - the discretization of $\boldsymbol{u}$ and s with shape functions N_I for node I is given by

$$\begin{aligned} \boldsymbol{u} &= \sum_{I=1}^{N} N_I \hat{\boldsymbol{u}}_I, & \underline{\boldsymbol{\varepsilon}} &= \sum_{I=1}^{N} [B_I^{\boldsymbol{u}}]\hat{\boldsymbol{u}}_I\,, \\ s &= \sum_{I=1}^{N} N_I \hat{s}_I, & \nabla s &= \sum_{I=1}^{N} [B_I^{s}]\hat{s}_I\,, \end{aligned}$$

with

$$[B_I^{\boldsymbol{u}}] = \begin{bmatrix} N_{I,x} & 0 \\ 0 & N_{I,y} \\ N_{I,y} & N_{I,x} \end{bmatrix} \qquad \text{and} \qquad [B_I^{s}] = \begin{bmatrix} N_{I,x} \\ N_{I,y} \end{bmatrix}.$$

Inserting these discretizations into the left hand sides of Eq. (4) and Eq. (5), one obtains the residuals

$$\left[R_I\right] = \begin{bmatrix} R_I^{\boldsymbol{u}} \\ R_I^{s} \end{bmatrix} = \int_\Omega \begin{bmatrix} [B_I^{\boldsymbol{u}}]^T \underline{\boldsymbol{\sigma}} \\ N_I \dfrac{\dot{s}}{M} - [B_I^{s}]^T \boldsymbol{q} + N_I\left(s\,\underline{\boldsymbol{\varepsilon}}^T \cdot \underline{\mathbb{C}}\,\underline{\boldsymbol{\varepsilon}} + \dfrac{G}{2\,\epsilon}(s-1)\right) \end{bmatrix} dV\,.$$

The tangent matrix $\left[K_{IJ}\right]$ as well as the stiffness matrix $\left[D_{IJ}\right]$ are symmetric and given by

$$\left[K_{IJ}\right] = \int_\Omega \begin{bmatrix} [B_I^{\boldsymbol{u}}]^T (s^2+\eta)\, \underline{\mathbb{C}}\, [B_J^{\boldsymbol{u}}] & [B_I^{\boldsymbol{u}}]^T 2s\, \underline{\mathbb{C}}\, \underline{\boldsymbol{\varepsilon}} N_J \\ N_I 2s (\underline{\mathbb{C}}\, \underline{\boldsymbol{\varepsilon}})^T [B_J^{\boldsymbol{u}}] & 2G\,\epsilon\, [B_I^s]^T [B_J^s] + N_I \left(\underline{\boldsymbol{\varepsilon}}^T \cdot \underline{\mathbb{C}}\, \underline{\boldsymbol{\varepsilon}} + \frac{G}{2\,\epsilon} \right) N_J \end{bmatrix} dV$$

and

$$\left[D_{IJ}\right] = \int_\Omega \begin{bmatrix} 0 & 0 \\ 0 & \frac{1}{M} N_I N_J \end{bmatrix} dV \,.$$

Gauss quadrature is used to evaluate the integrals and the time integration of the transient terms is done with the backward Euler method. An automatic step size control is helpful for the simulations because of the rapidly decreasing stiffness during fracture.

4 Results

The equations have been implemented into a quadrilateral plane strain element. Some results from simulations of different 2D problems are shown in this section. In all calculations isotropic material with Lamé constants $\lambda = \mu = 22\,\frac{\text{kN}}{\text{mm}^2}$ is considered. The scaling factor for the residual stiffness is $\eta = 10^{-5}$.

4.1 Mode I loading of a plate with initial crack

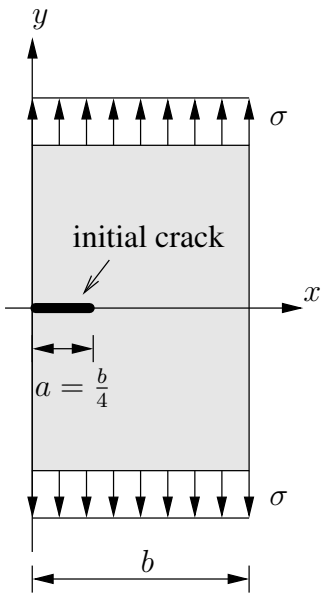

Figure 2: Experimental setup

Fig. 2 shows the setup for a plate ($b = 10$ cm) with an initial crack under mode I loading which is used in the numerical simulations of this section. Exploiting the symmetry of the sample only the upper half of the structure is considered in the numerical model. Near the crack a uniform quadratic grid of mesh size $h = 0.3125$ mm is used for the discretization. The system is initially unstrained and then loaded by a linearly increasing tension

$$\sigma(t) = \sigma_0 \cdot \frac{t}{t_0} \quad \text{with} \quad \frac{\sigma_0}{t_0} = 600\,\frac{\text{N}}{\text{cm}^2\text{sec}}\,.$$

The initial crack is modeled by setting $s(x, y)$ to zero, where $0 \le x \le a$ and $y = 0$. However, this manipulation of the s-field produces an unstable situation, which is an undesirable starting point for the simulations. Therefore one static iteration is performed to find a stress free, stationary state ($\dot{s} = 0$) to start from. The contour plots in Fig. 3 show the situation before and after the static iteration step for $\epsilon = 6$ mm. The initially sharp line which indicates the

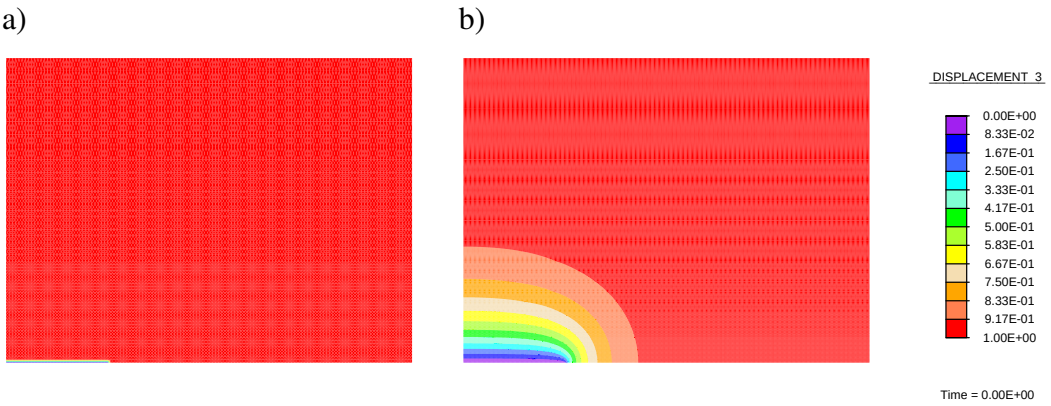

Figure 3: Contour plots of s a) before and b) after the starting step

crack in Fig. 3a) is smoothened in the stationary state shown in Fig. 3b). The parameter ϵ controls how much the initially sharp interface is smoothened in the static iteration step. This is illustrated in Fig. 4. The plot shows nodal values of s along the positive y-axis in the stationary state for different values of ϵ. If ϵ is sufficiently small, the values are in good agreement with the analytic results obtained from the 1D stationary example of section 2.1.

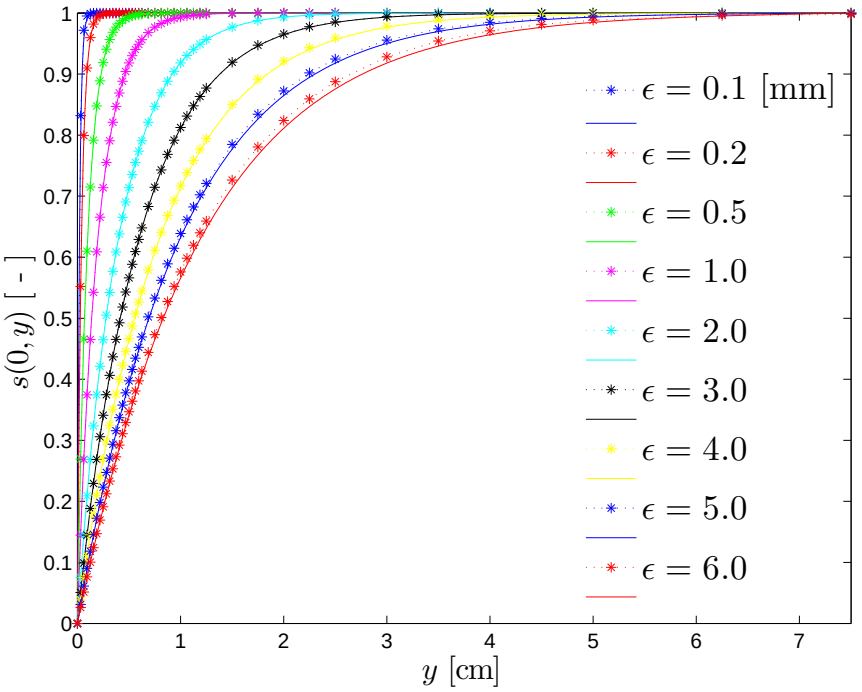

Figure 4: Nodal values of s (stars) along the y-axis for different values of ϵ compared to the analytic 1D solution (solid line)

For the setup shown in Fig. 2 an analytical solution in terms of stress intensity factors is available in [9]:

$$K_I = \sigma\sqrt{\pi a}\sqrt{\frac{2b}{\pi a}\tan\left(\frac{\pi a}{2b}\right)}\cdot C\left(\frac{a}{b}\right) \tag{6}$$

with

$$C\left(\frac{a}{b}\right) = \frac{0.752 + 2.02\frac{a}{b} + 0.37\left(1-\sin\left(\frac{\pi a}{2b}\right)\right)^3}{\cos\left(\frac{\pi a}{2b}\right)}\,.$$

According to Griffith's criterion a crack will grow if the released strain energy is large enough to form the new crack surfaces. In a plane strain setting Griffith's crack growth criterion [10] reads

$$\frac{1-\nu^2}{E}\,K_I^2 \geq G\,. \tag{7}$$

From Eq. (7) together with Eq. (6) the critical value σ_{crit} for the mode I stress load is given by

$$\sigma_{\text{crit}} = \sqrt{\frac{E}{1-\nu^2}\,\frac{G}{2b\,\tan\left(\frac{\pi a}{2b}\right)}}\cdot C\left(\frac{a}{b}\right)^{-1}\,.$$

In the numerical simulation the stress load increases linearly with time and the crack growth should start at time $t_{\text{crit}} = \frac{\sigma_{\text{crit}}}{\sigma_0}\,t_0$. Fig. 5 shows how the numerical simulations compare with the analytical results for Griffith's model. Here the lengthscale parameter ϵ and the mobility constant M are

$$\epsilon = 0.625\,\text{mm} \qquad \text{and}$$

$$M = 5.0\,\frac{\text{cm}^2}{\text{N}\cdot\text{sec}}.$$

The crack resistance G is varied from 0.25 to $10.0\,\frac{\text{N}}{\text{mm}}$. The start of crack propagation is defined as the time when the s-value of the first node in front of the initial crack becomes zero. With the chosen values for the parameters ϵ and M the numerical values for the start of crack propagation lie close to the analytic curve from the Griffith criterion.

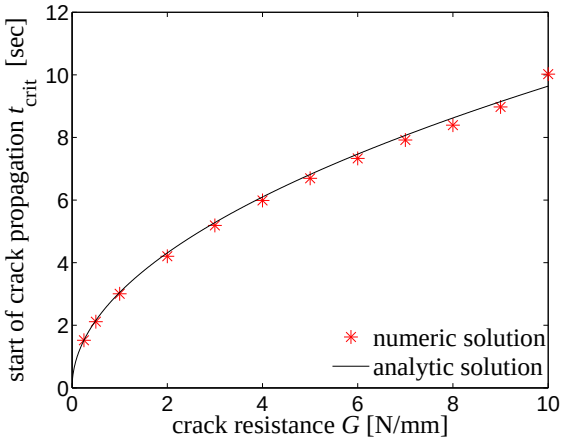

Figure 5: Start of crack propagation for different values of G (stars) compared to the analytic solution (solid line)

4.2 Influence of the mobility parameter M

The same example as in section 4.1 was chosen to study the influence of the mobility constant M on the crack propagation behaviour. The parameter ϵ and the crack resistance G are held constant at

$$\epsilon = 0.625\,\text{mm} \qquad \text{and} \qquad G = 1.0\,\frac{\text{N}}{\text{mm}}\,,$$

whereas the mobility M is varied in a range from 0.01 to $10\,\frac{\text{cm}^2}{\text{N·sec}}$.

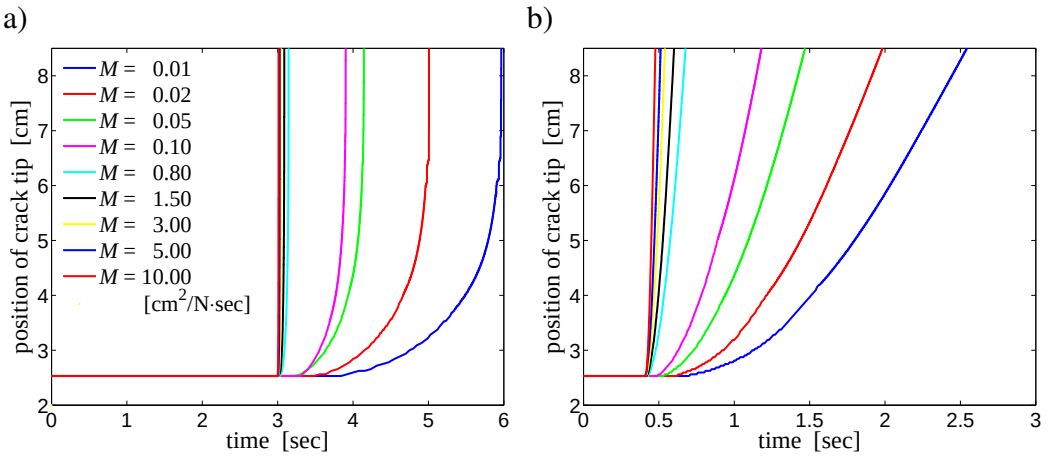

Figure 6: Position of the crack tip versus time for a) stress load and b) displacement load

To track the crack tip the nodal values of the crack field s along the positive x-axis are recorded. The node with the largest x-coordinate where s equals zero is defined as the crack tip position.

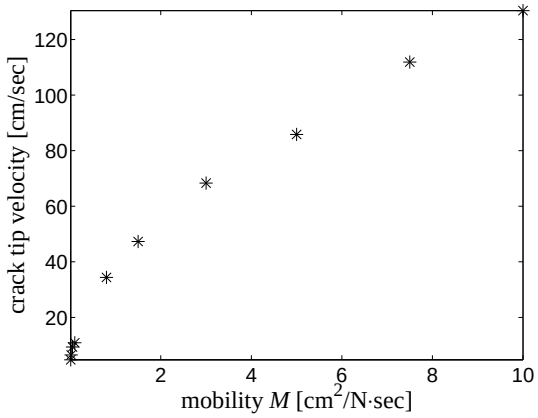

Figure 7: Crack tip velocity versus mobility M

The two plots of Fig. 6 show curves describing the crack tip position as a function of time for different values of M. The same stress load as in the previous calculations was used in the simulations for Fig. 6a), whereas in the simulations for Fig. 6b) a linearly increasing displacement load was applied instead of the stress load. Similarly for both loading cases, small values of M significantly delay the start of the crack propagation.

In the stress loading case (Fig. 6a) the crack grows instantaneously at time $t \approx 3$ sec for any sufficiently large M. In this case the solution can be considered as stationary. In the transient solutions for smaller values of M, the crack tip velocity immediately after the start of the crack propagation is significantly dependent on M. However, after this starting phase, when the crack tip reaches the middle of the sample $x \approx 5$ cm the further cracking is also instantaneous.

In the displacement load simulations (Fig. 6b), stable crack growth can be observed and the crack tip velocity can be measured by finding the slope of the curve. After the crack tip passes $x = 5$ cm the velocity can be regarded as constant. A linear regression analysis of the curves where the crack tip position is between 5.0 and 8.5 cm gives the velocities shown in Fig. 7.

4.3 Mode I loading of a plate with circular hole

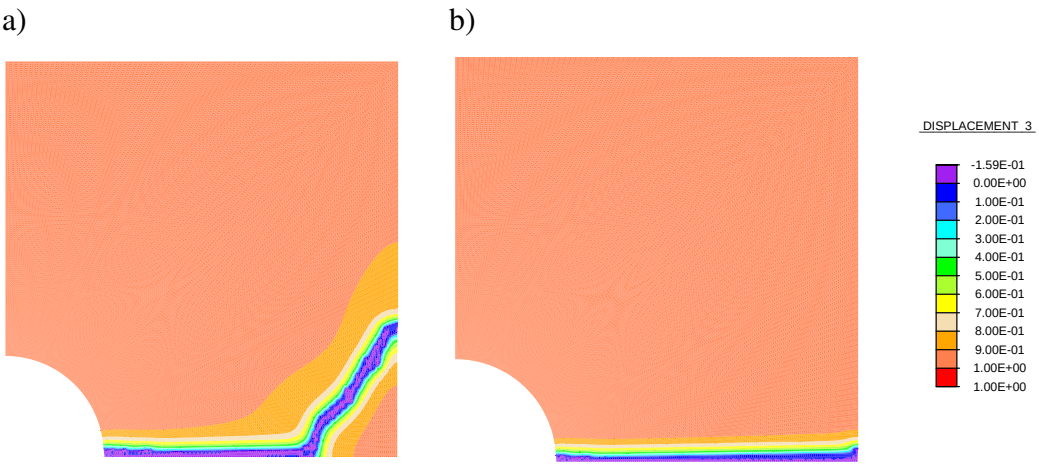

Figure 8: Contour plots of s a) for $G = 0.25\frac{\text{N}}{\text{mm}}$ b) for $G = 1.0\frac{\text{N}}{\text{mm}}$.

In this simulation an initially undamaged plate (20×20 cm) with a circular hole of radius $r = 2.5$ cm under a mode I displacement load is considered. The stiffness parameters λ, μ, and η are the same as in the previous examples. The mobility constant is set to $M = 5\,\frac{\text{cm}^2}{\text{N}\cdot\text{sec}}$. Again, exploiting the symmetry of the structure, the numerical model consists of only one quarter of the plate. 150×150 elements are used for the discretization and the length parameter ϵ is 1 mm. Fig. 8 shows contour plots of s of the fully cracked plate for $G = 0.25\frac{\text{N}}{\text{mm}}$ and $G = 1.0\frac{\text{N}}{\text{mm}}$, respectively. In both cases the crack initiates at the place of highest stress concentration, i.e. at the hole. With further increased loads the crack propagates in horizontal direction. In case of the lower value for G (Fig. 8a), the crack branches before the plate is fully cracked, whereas no branching occurs for $G = 1.0\frac{\text{N}}{\text{mm}}$ (Fig. 8b). This is due to the fact that for higher values of G more energy is needed to create new crack surfaces.

5 Summary

Minimization of the total energy with respect to the displacement field and the crack field is the basic principle of Bourdin's regularized fracture model. Contrary to [2, 3, 11] where the minimization is performed with an alternate minimizations algorithm, we interpret the crack variable as the order parameter of a phase field model and address cracking as a phase transition problem. Therefore a Ginzburg-Landau type evolution equation and an additional parameter, the mobility M, had to be introduced to the model. The influence of this newly introduced constant on the crack propagation behaviour has been explored in a simple mode I simulation. Sufficiently large values produce quasi-stationary solutions which are in good agreement with the classical Griffith model, while small values of M significantly delay the crack propagation. Extending the scope of Griffith's model, our phase field formulation, as well as Bourdin's model, needs no extra criterion to simulate crack initiation and branching.

References

[1] G.A. Francfort, J.-J. Marigo, Revisiting brittle fracture as an energy minimization problem, J. Mech. Phys. Solids 46 (8) (1998) 1319-1342

[2] B. Bourdin, Numerical implementation of the variational formulation of quasi-static brittle fracture, Interfaces Free Bound. 9 (2007) 411-430

[3] B. Bourdin, G.A. Francfort, J.-J. Marigo, The variational approach to fracture, J. Elasticity 91 (2008) 5-148

[4] A. Braides, Γ-convergence for Beginners, Oxford University Press, Oxford, 2002

[5] L. Eastgate et al., Fracture in mode I using a conserved phase-field model, Phys. Rev. E 71 (2002) 036117

[6] R. Spatschek et al., Phase field modeling of fast crack propagation, Phys. Rev. Lett. 96 (2006) 015502

[7] R. Spatschek et al., Phase field modeling of fracture and composite materials, Proceedings of CDCM 2008, Stuttgart

[8] V. Ginzburg, L. Landau, On the theory of superconductivity, Zh. Eksp. Teor. Fiz. 20 (1950) 1064-1082

[9] D. Gross, T. Seelig, Fracture Mechanics, Springer, Berlin, Heidelberg, New York, 2006

[10] A. Griffith, The phenomena of rupture and flow in solids, Phil. Trans. Roy. Soc. London 221 (1921) 163-198

[11] G. Del Piero, G. Lancioni, R. March, A variational model for fracture: numerical experiments, J. Mech. Phys. Solids 55 (2007) 2513-2537